

Technical Report Documentation Page

1. Report No.	2. Government Accession No.	3. Recipient's Catalog No.	
4. Title and Subtitle		5. Report Date	
		6. Performing Organization Code	
7. Author(s)		8. Performing Organization Report No.	
9. Performing Organization Name and Address		10. Work Unit No. (TRAIS)	
		11. Contract or Grant No.	
12. Sponsoring Agency Name and Address		13. Type of Report and Period Covered	
		14. Sponsoring Agency Code	
15. Supplementary Notes			
16. Abstract			
17. Key Words		18. Distribution Statement	
19. Security Classif. (of this report) Unclassified	20. Security Classif. (of this page) Unclassified	21. No. of Pages	22. Price

Distributed heat release effects on entropy generation by premixed, laminar flames

Akbar Laksana¹ , Parth Patki¹, Tony John²,
Vishal Acharya²  and Timothy Lieuwen^{1,2}

International Journal of Spray and
Combustion Dynamics
1–8

© The Author(s) 2023

Article reuse guidelines:

sagepub.com/journals-permissions

DOI: 10.1177/17568277231172887

journals.sagepub.com/home/scd



Abstract

This article studies the generation of entropy disturbances by laminar premixed flames. The total entropy generation equals the integrated ratio of the local heat release rate and the local temperature, namely, $\int (\dot{q} / T) dV$. Due to this path dependency, evaluating this integral requires an understanding of how the heat release is distributed in the temperature space. Several studies evaluate the local entropy generation as $(\int \dot{q} dV) / T_b$, where T_b refers to the burned gas temperature, implicitly assuming all the heat release occurs at T_b . Such an approximation is motivated by the high activation energy nature of combustion chemistry. This work evaluates this assumption by comparing it to results from one-dimensional premixed flame calculations for hydrogen, methane, and propane-air flames over a range of pressures, equivalence ratios, and preheat temperatures, quantified via the ratio κ . We show that this assumption is quite reasonable for methane and propane-air flames (with errors ranging from 5% to 25%) but deviates significantly from the exact results for hydrogen flames (where errors can be as high as 50%). In general, the peak heat release moves to lower temperatures as preheat temperature is increased. Noting that the temperature sensitivity of heat release is directly related to the activation energy, we use Law's approach to extract global activation energies and show that the deviations of κ from unity can be approximately correlated with β_{eff} . Finally, we show that significant improvements in entropy generation calculations can be obtained by estimating $\int (\dot{q} / T) dV$ using $(\int \dot{q} dV) / T_{\text{peak}}$, where T_{peak} is the temperature at which the reaction rate peaks. This estimation leads to predictions of $\sim 5\%$ within the exact value for the hydrocarbon cases but can still be in significant error for hydrogen at certain conditions.

Keywords

Entropy generation, chemical heat release, heat release distribution

Date received: 21 February 2023; accepted: 4 April 2023

1. Introduction

Sound generation from combustion can be classified into direct and indirect noise. Direct combustion noise is generated by fluctuations in reaction rate, leading to fluctuations in heat release and species molar production rates. Indirect noise occurs when entropy disturbances generated by the flame are accelerated in the nozzle at the combustor exit.^{1,2} The objective of this article is to analyze the entropy generation from the heat release of a laminar premixed flame. In general, entropy disturbances stem from a variety of sources, which for a perfect gas is governed by the equation:³

$$\rho T \frac{Ds}{Dt} = -\nabla \cdot \vec{q} + \underline{\underline{\tau}} : (\nabla \vec{u}) - \rho \sum_{i=1}^N \mathcal{D}_i \nabla Y_i \cdot \vec{F}_i - \sum_{i=1}^N \frac{\mu_i}{MW_i} [\dot{w}_i + \nabla \cdot (\rho \mathcal{D}_i \nabla Y_i)] \quad (1)$$

This equation shows the entropy of a fluid mass is affected by diffusion, body forces, and chemical reaction. In combustion applications with strongly exothermic reactions, the unsteady reaction rate terms are well known to be the dominant term. For example, Nishida et al.⁴ compared the magnitudes of these source terms for premixed methane and hydrogen

¹George W. Woodruff School of Mechanical Engineering, Georgia Institute of Technology, Atlanta, GA, USA

²Daniel Guggenheim School of Aerospace Engineering, Georgia Institute of Technology, Atlanta, GA, USA

Corresponding author:

Vishal Acharya, Daniel Guggenheim School of Aerospace Engineering, Georgia Institute of Technology, 270 Ferst Drive, Atlanta, GA 30332, USA.

Email: vishal@aerospace.gatech.edu

flames, showing that the chemical reaction terms are the dominant source of entropy production (second last term in the RHS). The chemical reaction source term can itself be decomposed as:

$$-\sum_{i=1}^N \frac{\mu_i}{MW_i} \dot{w}_i = \dot{q} - \sum_{i=1}^N \dot{w}_i \int_{T_0}^T c_{p,i} dT + \sum_{i=1}^N T s_i \dot{w}_i \quad (2)$$

Here, the RHS of equation (2) comprises chemical heat release rate, sensible enthalpy, and partial entropy term, respectively, i.e., exothermic reactions generate entropy not only via heat release, but also because of changes in number of moles and changes in composition. Further studies by Patki et al.⁵ showed that the chemical heat release term is the dominant one for air-breathing combustion systems, motivating the focus of this study. Retaining only the dominant heat release source term leads to equations (3) and (4), where u_s is the velocity of the boundary volume.

$$\rho \frac{D(s)}{Dt} = \frac{\partial(\rho s)}{\partial t} + \nabla \cdot (\rho \vec{u} s) = \frac{\dot{q}}{T} \quad (3)$$

$$\frac{d}{dt} \int_{V(t)} \rho s dV + \int_{A(t)} \rho s (\vec{u} - \vec{u}_s) \cdot \hat{n} dA = \int_{V(t)} \frac{\dot{q}}{T} dV \quad (4)$$

In the analysis of thermoacoustic instabilities, a flame model is included as part of a larger system model.⁶ The right-hand side of equation (4) equates the flame's entropy production. The further evolution of these disturbances and conversion to sound are a function of downstream flow and combustor geometry—which is not a focus of this article. In a preceding study,⁷ this right-hand term of equation (4) is estimated as:

$$\int \frac{\dot{q}}{T} dV \sim \frac{1}{T_b} \int \dot{q} dV \quad (5)$$

In other words, it is estimated as the spatially integrated heat release divided by the adiabatic flame temperature, T_b , which implicitly assumes that all the heat release occurs at T_b . However, this term is a path-dependent quantity that is a function of the temperature-weighted heat release. Moreover, detailed kinetic studies of flame structure clearly demonstrate that heat release is nonetheless distributed over a range of temperatures and nonnegligible heat release may occur at intermediate temperatures, such as with hydrogen.⁸ The objective of this study is to quantify the accuracy of the approximation in equation (5) as well as develop corrections to it.

2. Methodology and modeling approaches

The key quantity of interest to this article is the ratio κ_b , expressed in equation (6). κ_b is the ratio of entropy

generation from a flame where all the heat release occurs at T_b to that from a distributed heat release source.

$$\kappa_b = \frac{\frac{1}{T_b} \int \dot{q} dx}{\int \frac{\dot{q}}{T} dx} \quad (6)$$

This parameter κ_b is less than unity and converges to 1 as the heat release concentrates at $T = T_b$. For reasons discussed later, an alternative approach for calculating κ is with κ_p as shown in equation (7). Here, T_{peak} is the temperature at which the heat release rate peaks. Note that κ_p can have values exceeding unity since some heat release occurs at $T > T_{peak}$.

$$\kappa_p = \frac{\frac{1}{T_{peak}} \int \dot{q} dx}{\int \frac{\dot{q}}{T} dx} \quad (7)$$

Various approaches can be used to estimate the functional relationship between heat release rate and temperature needed to evaluate these integrals. We use two approaches, a model profile to obtain further insight and detailed kinetics calculations.

2.1. Model heat release profile

Some insight into the characteristics of this integral for combustion-type reactions can be obtained by considering a model heat release rate profile:^{9,10}

$$\omega(\theta) = B(1 - \theta)(e^{-\beta(1-\theta)} - e^{-\beta}) \quad (8)$$

Here, $\beta = \frac{E_a}{RT_b} \left(1 - \frac{T_u}{T_b}\right)$ is the Zeldovich number, while E_a is the activation energy, R is the gas constant, and T_u is the unburned or preheat temperature. $\omega = \frac{\dot{q}(\theta)}{Q}$ is the normalized heat release rate, Q is the integrated heat release, $\theta = \frac{T - T_u}{T_b - T_u}$ is the normalized temperature, and B

is a scaling parameter such that $\int_0^1 \omega(\theta) d\theta = 1$ resulting in $B = \beta^2 / \left(1 - e^{-\beta} \left(1 + \beta + \frac{\beta^2}{2}\right)\right)$. Figure 1 illustrates the variation in the distribution of the source function as a function of β for this model profile.

It shows that with increasing values of β , two effects occur—the heat release profile becomes more concentrated and the temperature of peak heat release, T_{peak} , shifts closer to the burned gas temperature. For this simple heat release model, both effects are proportional to β . We briefly consider the entropy generation associated with this model profile in the limit of large β . We can transform the integral form of equations (6) and (7) as:

$$\int \frac{\dot{q}}{T} dx = \int \frac{\dot{q}}{T} \left| \frac{dx}{dT} \right| dT = \int \frac{\dot{q}}{T} J dT \quad (9)$$

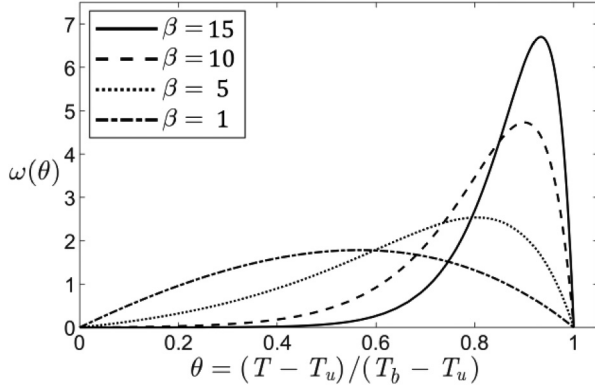


Figure 1. Illustration of source function given by equation (8) for different β .

where $J = |dx/dT|$. Evaluating the integration by parts using this new definition, we have equation (10):

$$\int_{T_u}^{T_b} \frac{\dot{q}}{T} dx = \frac{J(1)}{T_b \beta} + \frac{2}{\beta^2} \left[\frac{J(1)}{T_b^2} (T_b - T_u) - \frac{1}{T_b} \frac{dJ(1)}{d\theta} \right] + \mathcal{O}\left(\frac{1}{\beta^3}\right) \quad (10)$$

Note that $T(1) = T_b$, $J(1)$ is $|dx/dT|$ when $\theta=1$, and $dT/d\theta = (T_b - T_u)$. Following the same method from equation (10), with the approximation at high activation energy (or large β), yield equation (11).

$$\frac{1}{T_b} \int_{T_u}^{T_b} \dot{q} dx = \frac{J(1)}{T_b \beta} - \frac{2}{T_b \beta^2} \frac{dJ(1)}{d\theta} + \mathcal{O}\left(\frac{1}{\beta^3}\right) \quad (11)$$

This article also explores using $T_{peak} = T_b - \frac{(T_b - T_u)}{\beta}$, instead of dividing by T_b :

$$\frac{1}{T_{peak}} \int_{T_u}^{T_b} \dot{q} dx = \frac{J(1)}{T_b \beta} + \frac{J(1)}{T_b \beta^2} (T_b - T_u) - \frac{2}{T_b \beta^2} \frac{dJ(1)}{d\theta} + \mathcal{O}\left(\frac{1}{\beta^3}\right) \quad (12)$$

A few observations emerge from equation (10–12), which describes the expressions for the temperature-weighted integral. First, the exact expression, shown in equation (10), and the two approximate expressions, shown in equations (11) and (12), are identical to the leading order. Second, the leading order error of the two approximate expressions from the exact one is of $\mathcal{O}(1/\beta^2)$. Third, equation (12) shows that using T_{peak} yields a closer approximation of the exact result; i.e., utilizing T_{peak} is a more accurate approach than T_b , but both approaches differ from the exact result in order $1/\beta^2$. All these conclusions were expected but allow one to see them formally.

2.2. Detailed kinetic calculations

A more accurate way of describing the heat release is to use detailed kinetic calculations. This was done using a 1-D

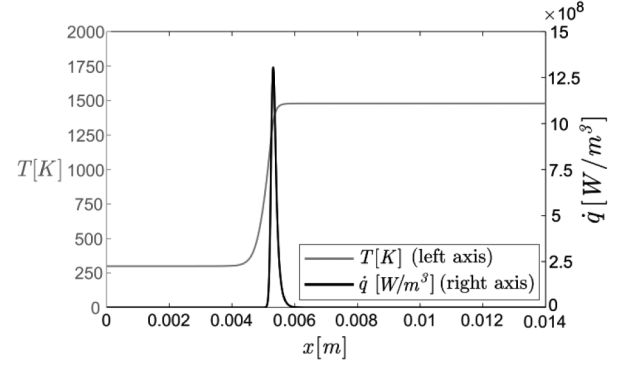


Figure 2. Heat release rate and temperature profile used in the integration of entropy ratio.

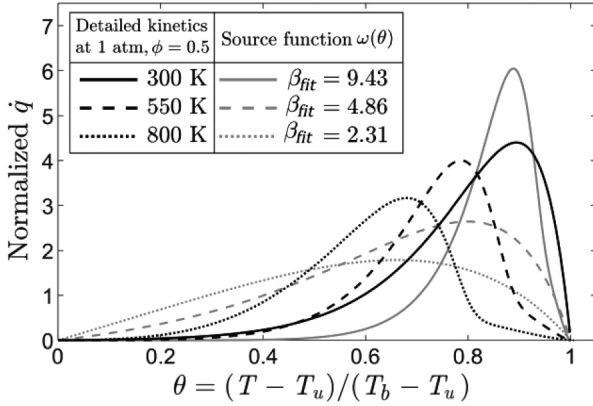
premixed, free flame model using Cantera.¹¹ Calculations were performed for hydrogen, methane, and propane-air systems. Methane-air combustion was modeled using GRI-Mech 3.0 mechanism¹² with 35 species and 325 reactions. Hydrogen-air combustion was modeled using UCSD mechanism¹³ with 57 species in 268 reactions. Propane-air combustion was modeled using Peters' mechanism¹⁴ with 31 species in 107 reactions. Grid independence tests¹⁵ were performed to determine the grid density necessary to achieve a converged value of the integrals in equations (6) and (7). Figure 2 illustrates an example calculation showing the heat release rate and temperature profile for a CH₄-air premixed free flame case at 1 atm, equivalence ratio (ϕ) of 0.5, at 300 K preheat temperature. These calculations were repeated for a range of operating conditions, summarized in Table 1.

Plots of the dependence of heat release rate upon temperature are shown in Figure 3. The plots show both the profile from the detailed kinetics, as well as the model from equation (8). Magnitudes of β for the latter case were chosen to minimize the least squares difference between equation (8) and the computed profiles, also can be thought of as quantifying an effective activation energy value for the detailed kinetics cases, denoted here as β_{fit} . Note that the heat release profiles are narrower in temperature space for the detailed kinetic calculations than the model profiles at lower β and behaving inversely at higher β . The value of the β parameter greatly influences the degree of heat release concentration when using the model of equation (8). A better fit between the model profiles and detailed kinetics can be obtained by using higher-order fitting functions but not further explored.

As discussed above, the value of β has a significant impact on the distribution of heat release. As such, it is useful to develop an approach to estimate an “effective β value,” denoted β_{eff} , and to correlate it with κ values. The previous data shown in Figure 3 have demonstrated the least squares fit of the computed profiles to the model profile in equation (8) to extract β values. However, this

Table 1. Operating conditions for case calculations.

Control parameter	Value and unit
Pressure	1 to 20 atm
Preheat temperature	300 to 800 K
Equivalence ratio, ϕ	0.5 to 1
Mixtures	CH ₄ , H ₂ , and C ₃ H ₈ with air as oxidizer.

**Figure 3.** Temperature dependence of heat release profile from Cantera calculations (CH₄, 1 atm and $\phi = 0.5$) and model profiles from equation (8) with β values that minimize least squares residual for indicated computed cases.

approach will, by definition, lead to a strong correlation of β_{eff} and κ and will not lead to additional insight. An alternative approach that leads to independent calculations of β_{eff} and κ is to extract global activation energies from detailed kinetics results. For example, Law¹⁶ utilizes the following expressions to define a global activation energy based on the mass burning rate:

$$f^o \sim \exp(-E_a/2RT_b) \quad (13)$$

$$E_a = -2R \left[\frac{\partial \ln f^o}{\partial (1/T_b)} \right]_p \quad (14)$$

Here, f^o is the mass burning rate, equal to the product of the density and flame speed. Using the definition of β , we can relate the Zeldovich number with the burning flux and temperatures of the flame through:

$$\beta_{eff} = -2 \left[\frac{\partial \ln f^o}{\partial (1/T_b)} \right]_p \frac{1}{T_b} \left(1 - \frac{T_u}{T_b} \right) \quad (15)$$

This β_{eff} value is then estimated from the temperature sensitivity of the mass burning rate. We performed calculations of the mass burning rate over a range of temperatures around the values shown in the results to estimate this partial derivative. The partial derivative term was calculated using linear regression of the natural logarithmic of the mass burning rate at independent value of equivalence

ratio. From here, it is possible to extract the slope of the linear trends which in turn will be the value of the partial derivative terms.

3. Results and discussion

This section presents entropy generation results for a range of preheat temperatures, pressures, equivalence ratios, and fuel compositions. In general, these sensitivities are quite complex, due to the shifting chemical pathways as pressure or equivalence ratio vary.⁵ However, some general understanding of key dependencies can be obtained. For example, it can be anticipated that as T_{peak} approaches T_b , the approximation of equation (7) will grow in accuracy. Here, T_{peak} is defined as the temperature at which heat release peaks. Defining the following normalized temperature value, where $\theta_{peak} = 1$ when $T_{peak} = T_b$:

$$\theta_{peak} = (T_{peak} - T_u)/(T_b - T_u) \quad (16)$$

The values of θ_{peak} are greater or less than 0.5, corresponding to T_{peak} values that are closer to T_b and T_u , respectively. Figure 4 plots the dependence of the θ_{peak} upon β_{eff} . It shows that θ_{peak} values are systematically lower for hydrogen, for reasons discussed earlier. It also shows a general correlation between these quantities, i.e., higher global activation energies generally lead to higher θ_{peak} values. Note that each line at constant equivalence ratio and pressure sweeps out the $300 < T_u < 800$ range, with higher β_{eff} or θ_{peak} values corresponding to the lowest T_u .

Finally, θ_{peak} decreases as the equivalence ratio sweeps from lean to stoichiometric and at higher preheat temperature. The hydrocarbon flames have θ_{peak} values ranging from about 0.6 to 0.95, indicating that θ_{peak} is always closer, and sometimes quite close to T_b . Note, however, that some hydrogen cases do have θ_{peak} values less than 0.5, showing that equation (7) is a very poor approximation. We will refer to these results in interpreting the entropy generation ratio, or κ , calculations below.

Figure 5 provides a representative compilation of calculations for methane-air combustion showing the variation of κ_b with equivalence ratio and preheat temperature, at three pressures. It shows that κ_b values range between about 0.75 to 0.9; i.e., the error in the estimate of entropy generation is about 10% to 25%. For the methane-air case, it also shows that κ_b is highest at lower equivalence ratios, at elevated pressure, and at lower preheat temperatures (again, note the preheat temperature is being swept from $300 < T_u < 800$ on a given line as T_b increases).

A comparable set of calculations for hydrogen are shown in Figure 6. This plot shows that κ_b values are as low as ~ 0.5 , indicating that the approximate expression for entropy generation can be in error by as much as 50%. The largest deviations occur for the elevated preheat temperature case where, as shown in Figure 4, T_{peak} occurs

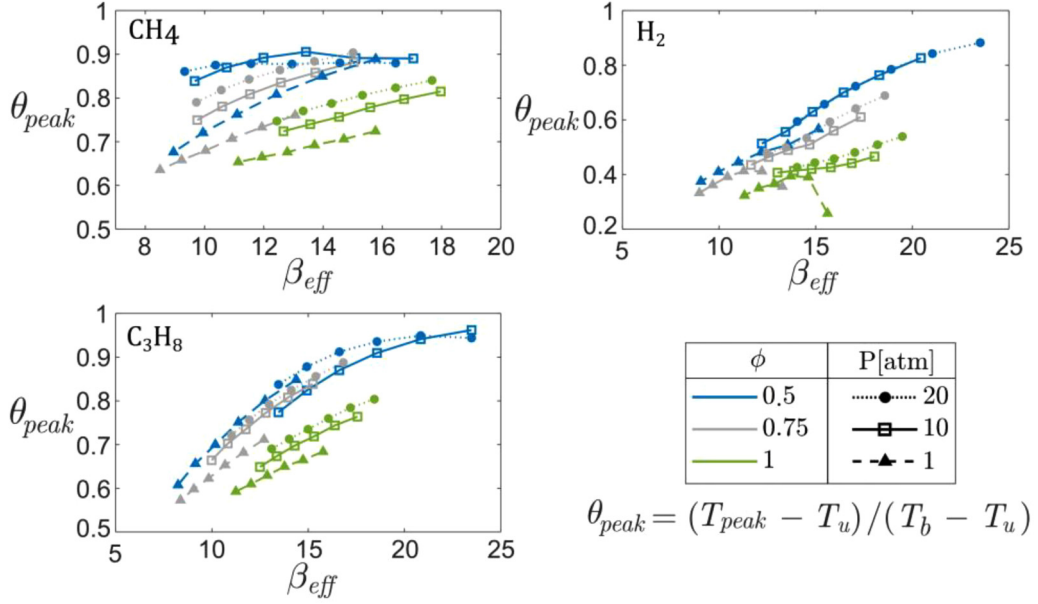


Figure 4. Dependence of normalized peak temperature upon β_{eff} for CH₄, H₂, and C₃H₈ at different conditions.

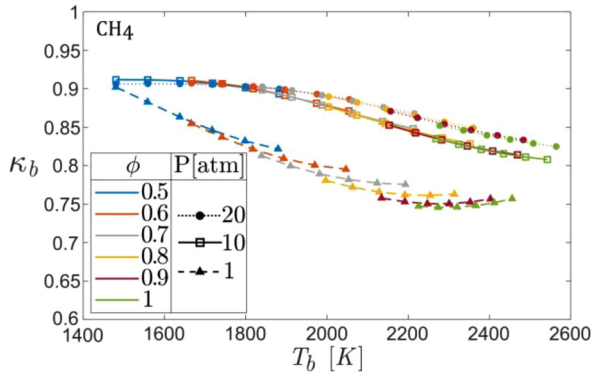


Figure 5. κ_b as a function of T_b for CH₄ at different conditions.

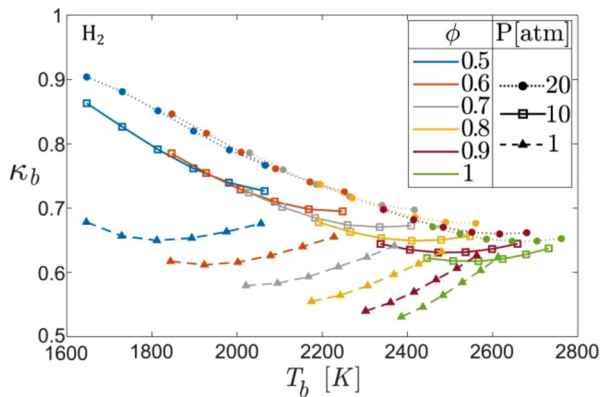


Figure 6. κ_b as a function of T_b for H₂ at different conditions.

closer to T_u than to T_b . Again, κ_b has the highest values under conditions of lower equivalence ratios, elevated pressure, and lower preheat temperature.

Although not plotted, κ_b ranges between 0.75 to 0.95 for propane-air combustion over the same set of conditions. Note that for both Figures 5 and 6, each curve contains results when the preheat temperature was varied from 300 to 800 K. The data points with the lowest T_b correlate to T_u value of 300 K and 800 K for the opposite.

We next consider methods for correlating the deviation of κ_b from unity using the effective activation energy. The value of β_{eff} was extracted using equation (15) for these same conditions. Figure 7 replots κ_b as a function of β_{eff} for most of the data shown in Figures 5 and 6. It shows some correlation, i.e., κ_b values are closer to unity for larger β_{eff} , but there is still considerable scatter. The propane data shows the clearest correlation, with the hydrogen data exhibiting the opposite trend for the 1 atm cases. Note also that the β_{eff} used here is a measure of the temperature sensitivity of the mass burning rate. However, it is also possible to identify the temperature sensitivities of other metrics (e.g., consumption rate of specific species, flame thickness, etc.) to compute a different β_{eff} .

It was noted earlier that using T_{peak} , rather than T_b will lead to better estimates for entropy generation. Figure 8 plots the dependence of κ_p upon β_{eff} . For methane-air case, the κ_p method is quite accurate; it yields a difference of up to 3% to 5% from the detailed kinetic calculation. Furthermore, this κ_p value is less sensitive to operating conditions (i.e., preheat temperature, pressure, and mixture composition) compared to the κ_b method of equation (6).

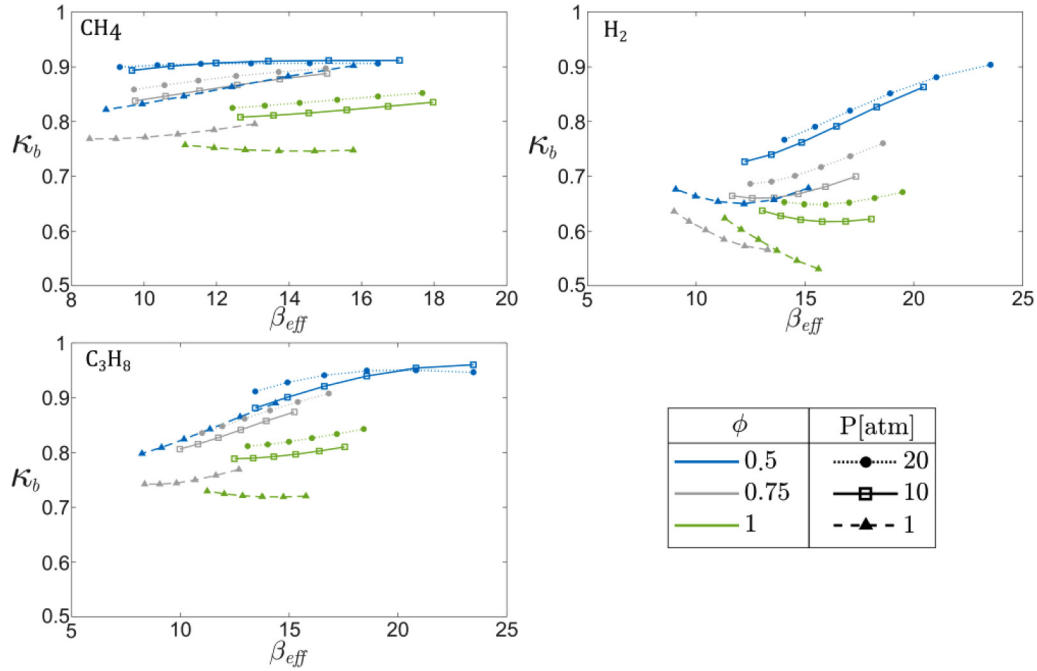


Figure 7. κ_b as a function of β_{eff} for CH_4 , H_2 , and C_3H_8 at different conditions.

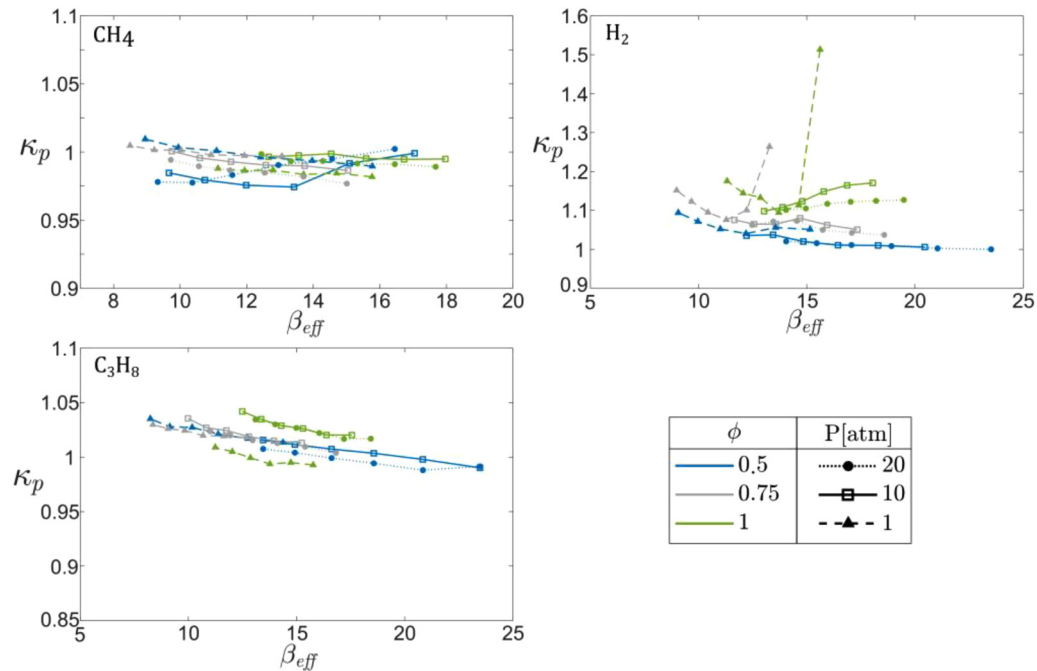


Figure 8. κ_p as a function of β_{eff} for CH_4 , H_2 , and C_3H_8 at different conditions.

The range of κ_p for hydrogen-air combustion is 1 to 1.5. The alternative method of estimating entropy generation using T_{peak} still yields a large error for hydrogen case, of up to 50%, especially at low-pressure.

To summarize these results—entropy generation from hydrocarbons can be estimated reasonably accurate by

assuming that the heat release occurs at T_b and substantial improvement can be obtained by further assuming that all heat release occurs at T_{peak} . However, these results indicate that more care is required in estimating entropy generation from hydrogen flames, and simple approximations based on either T_b or T_{peak} can lead to significant errors.

4. Conclusion

Entropy production by flames is a path-dependent quantity that is a function of the temperature-weighted heat release. It is a common assumption to assume that most of the heat release occurs at the burned gas temperature, and thereby to equate the flame's entropy production by $\frac{1}{T_b} \int \dot{q} dV$. This study shows that this approximation is a reasonable one for hydrocarbon flames and is further improved by using the temperature of peak heat release, T_{peak} , instead of, T_b . Estimating entropy generation for hydrogen flames requires further consideration since it can lead to significant error in certain cases when using either T_b or T_{peak} . This study also demonstrates that the deviation of this approximation from the exact result can be approximately correlated with a global activation energy.

Acknowledgments

This research was funded by the U.S. Federal Aviation Administration Office of Environment and Energy through ASCENT, the FAA Center of Excellence for Alternative Jet Fuels and the Environment, and Project 55 through FAA Award Number 13-C-AJFE-GIT-058 under the supervision of Roxanna Moores. Any opinions, findings, conclusions, or recommendations expressed in this material are those of the authors and do not necessarily reflect the views of the FAA.


Declaration of conflicting interests


The author(s) declared no potential conflicts of interest with respect to the research, authorship, and/or publication of this article.

Funding

The author(s) disclosed receipt of the following financial support for the research, authorship, and/or publication of this article: This research was funded by the U.S. Federal Aviation Administration Office of Environment and Energy through ASCENT, the FAA Center of Excellence for Alternative Jet Fuels and the Environment, Project 55 through FAA Award Number 13-C-AJFE-GIT-058 under the supervision of Roxanna Moores. Any opinions, findings, conclusions, or recommendations expressed in this material are those of the authors and do not necessarily reflect the views of the FAA.

ORCID iDs

Akbar Laksana  <https://orcid.org/0000-0001-9567-0725>

Vishal Acharya  <https://orcid.org/0000-0003-0143-7661>

References

1. Dowling AP and Mahmoudi Y. Combustion noise. *Proc Combust Inst* 2015; 35: 65–100.
2. Marble FE and Candel SM. Acoustic disturbance from gas non-uniformities convected through a nozzle. *J Sound Vib* 1977; 55: 225–243.

3. Lieuwen TC. Overview and basic equations. In: *Unsteady combustor physics*. Cambridge: Cambridge University Press, 2012, pp. 1–16.
4. Nishida K, Takagi T and Kinoshita S. Analysis of entropy generation and exergy loss during combustion. *Proc Combust Inst* 2002; 29: 869–874.
5. Patki P, Acharya V and Lieuwen T. Entropy generation mechanisms from exothermic chemical reactions in laminar, premixed flames. *Proc Combust Inst* 2022. Epub ahead of print 23 October 2022. DOI: 10.1016/J.PROCI.2022.08.069.
6. Huber A and Polifke W. Dynamics of practical premixed flames, part I: model structure and identification. *Int J Spray Combust Dyn* 2009; 1: 199–228.
7. John T, Acharya V and Lieuwen T. Entropy transfer functions of externally forced flames. In: *Spring technical meeting, eastern states section of the combustion institute*. Pittsburgh, PA: The Combustion Institute, 6–9 March 2022, p. 3. Paper no. 149LF-0075.
8. Dasgupta D, Sun W, Day M, et al. Effect of turbulence–chemistry interactions on chemical pathways for turbulent hydrogen–air premixed flames. *Combust Flame* 2017; 176: 191–201.
9. Benguria RD, Cisternas J and Depassier MC. Variational calculations for thermal combustion waves. *Phys Rev E* 1995; 52: 4410–4413.
10. Clavin P and Liñán A. Theory of gaseous combustion. In: Velarde MG (ed) *Nonequilibrium cooperative phenomena in physics and related fields*. Boston, MA: Springer US, 1984, pp. 291–338.
11. Goodwin DG, Speth RL, Moffat HK, et al. Cantera: an object-oriented software toolkit for chemical kinetics, thermodynamics, and transport processes (2.5.1), <https://www.cantera.org> (2021).
12. Smith GP, Golden DM, Frenklach M, et al. GRI 3.0 mechanism, http://www.me.berkeley.edu/gri_mech/.
13. Chemical-kinetic mechanisms for combustion applications, San Diego mechanism web page, mechanical and aerospace engineering (combustion research), University of California at San Diego, <http://combustion.ucsd.edu>.
14. Jerzembeck S, Peters N, Pepiot-Desjardins P, et al. Laminar burning velocities at high pressure for primary reference fuels and gasoline: experimental and numerical investigation. *Combust Flame* 2009; 156: 292–301.
15. Felden A. *CANTERA tutorials, a series of tutorials to get started with the python interface of Cantera version 2.1.1*. November 2015.
16. Law CK. Laminar premixed flames. In: *Combustion physics*. Cambridge: Cambridge University Press, 2006, pp. 234–302.

Nomenclature

A	Area
B	Scaling parameter
c_p	Constant pressure-specific heat
D	Diffusion coefficient
E_a	Activation energy
\vec{F}	Body forces per unit mass
f°	Burning flux

m	Number of flame points
MW	Molecular weight
p	Pressure
Q	Integrated heat release rate
\bar{q}	Heat flux
\dot{q}	Heat release rate
R	Gas constant
s	Specific entropy
T	Temperature
t	Time
u	Velocity
V	Volume
\dot{w}	Mass-based production rate
x	Flame location
Y	Mass fraction

Greek Symbols

β	Zeldovich number
ρ	Density

$\underline{\tau}$	Shear stress
$\underline{\mu}$	Molar chemical potential
ϕ	Equivalence ratio
ω	Normalized heat release rate
θ	Normalized temperature
κ	Chemical heat release entropy generation ratio

Subscripts

b	Burned/adiabatic flame
eff	Effective, used to denote Zeldovich number extracted with Law's method ¹⁶
fit	Function fit, used to denote Zeldovich number extracted with source function fit of equation (8).
i	Species i
p	Peak
u	Unburned
0	Initial